J|A|C|S
ARTICLES
Published on Web 08/17/2006

Rational Synthesis, Self-Assembly, and Optical Properties of PbS−Au Heterogeneous Nanostructures via Preferential Deposition

Jian Yang,[†] Hendry Izaac Elim,[‡] QingBo Zhang,[§] Jim Yang Lee,*[,†,§] and Wei Ji[‡]

Contribution from the Molecular Engineering of Biological and Chemical Systems (MEBCS), Singapore-MIT Alliance, E4-04-10, 4 Engineering Drive 3, Singapore 117576, Department of Physics, 2 Science Drive 3, National University of Singapore, Singapore 117542, and Department of Chemical and Biomolecular Engineering, National University of Singapore, 4 Engineering Drive 3, Singapore 117576

Received April 11, 2006; E-mail: cheleejy@nus.edu.sg

Abstract: High-quality, monodisperse PbS−Au_1, PbS−Au_4, and PbS−Au_n nanostructures have been synthesized via a facile and convenient solution chemistry approach. HRTEM images of these nanostructures showed good selectivity of gold deposition on the semiconductor in several spatially correlated directions. The formation of these regular nanostructures can be explained by the difference in polarity of crystal facets that led to the selective growth of metal on the semiconductor surface. Owing to their narrow size distribution and intrinsic high-symmetry, the resulting PbS−Au_4 and PbS−Au_n heterogeneous nanostructures could spontaneously self-assemble into ordered arrays with different symmetries. From the results of the pump−probe measurements, the presence of Au in PbS−Au_4 nanostructures has substantially altered the nonlinear optical response of PbS nanocrystals.

Introduction

Fabrication of high-quality and monodisperse nanocrystals consisting of discrete domains of different materials is the natural next step in the development of nanomaterials,[1−4] after the remarkable success in growing single-component nanocrystals with controlled dimensions and intriguing morphologies.[5−7] The lure of nanostructured composites is that they can integrate several different functionalities required by the applications in one common structure, which are otherwise difficult to accomplish in single component materials.[8] Furthermore, the close coupling of different components on the nanoscale may significantly improve the application performance, or even create new properties.[9,10] Semiconductor/metal nanocomposites are a classic example. It has been well documented that metal nanoparticles on the surface of semiconductors can improve the charge separation in semiconductors and subsequently enhance the photocatalytic activities of the latter.[10] Metal nanoparticles in these nanostructures can also alter the optical properties of the semiconductors, particularly in photoluminescence quenching or enhancement.[1,11] Such effects can be used to advantage in chemical and biochemical sensing. However, it remains to be a great challenge to produce nanoscale heterostructures, especially those with extended order and hierarchy, from materials differing significantly in crystal structures and chemical properties. While the literature is replete with specific recipes, a rational approach to multicomponent material design is anytime more valuable and highly desirable.

Recently, Banin's group reported the solution growth of gold tips on hexagonal-phase CdSe nanorods at room temperature.[1] This selective growth of metal on semiconductor nanocrystals is totally different from the epitaxial growth observed in many other papers.[12] In a follow-up work the selective growth of gold on hexagonal-phase CdSe nanocrystals was also demonstrated by the same group,[13] as shown in Scheme 1a. The selective

[†] Singapore-MIT Alliance.
[‡] Department of Physics, National University of Singapore.
[§] Department of Chemical and Biomolecular Engineering, National University of Singapore.

(1) Mokari, T.; Rothenberg, E.; Popov, I.; Costi, R.; Banin, U. *Science* **2004**, *304*, 1787.
(2) Paholski, C.; Kornowski, A.; Weller, H. *Angew. Chem., Int. Ed.* **2004**, *43*, 4774.
(3) Yu, H.; Chen, M.; Rice, P. M.; Wang, S. X.; White, R. L.; Sun, S. *Nano Lett.* **2005**, *5*, 379. Li, Y.; Zhang, Q.; Nurmikko, A. V.; Sun, S. *Nano Lett.* **2005**, *5*, 1689.
(4) Pellegrino, T.; Fiore, A.; Carlino, E.; Giannini, C.; Cozzoli, P. D.; Ciccarella, G.; Respaud, M.; Palmirotta, L.; Cingolani, R.; Manna, L. *J. Am. Chem. Soc.* **2006**, *128*, 6690. Gu, H.; Zheng, R.; Zhang, X.; Xu, B. *J. Am. Chem. Soc.* **2004**, *126*, 5664.
(5) Xia, Y. N.; Yang, P. D.; Sun, Y. G.; Wu, Y. Y.; Mayers, B.; Gates, B.; Yin, Y. D.; Kim, F.; Yan, Y. Q. *Adv. Mater.* **2003**, *15*, 353.
(6) Peng, X. G.; Manna, L.; Yang, W. D.; Wickham, J.; Scher, E.; Kadavanich, A.; Alivisatos, A. P. *Nature* **2000**, *404*, 59. Pradhan, N.; Goorskey, D.; Thessing, J.; Peng, X. G. *J. Am. Chem. Soc.* **2005**, *127*, 17586. Yu, S. H.; Antonietti, M.; Colfen, H.; Giersig, M. *Angew. Chem., Int. Ed.* **2002**, *41*, 2356.
(7) Chen, C. C.; Yeh, C. C. *Adv. Mater.* **2000**, *12*, 738. Yang, J.; Xue, C.; Yu, S. H.; Zeng, J.; Qian, Y. *Angew. Chem., Int. Ed.* **2002**, *41*, 4697. Yang, J.; Zeng, J. H.; Yu, S. H.; Yang, L.; Zhou, G.; Qian, Y. T. *Chem. Mater.* **2000**, *12*, 3259.
(8) Sanchez, C.; Lebeau, B.; Chaput, F.; Boilot, J. P. *Adv. Mater.* **2003**, *15*, 1969.
(9) Robel, I.; Bunker, B. A.; Kamat, P. V. *Adv. Mater.* **2005**, *17*, 2458.
(10) Hirakawa, T.; Kamat, P. V. *J. Am. Chem. Soc.* **2005**, *127*, 3928.
(11) Lin, H. Y.; Chen, Y. F.; Wu, J. G.; Wang, D. I.; Chen, C. C. *Appl. Phys. Lett.* **2006**, *88*, 161911.
(12) Shi, W.; Zeng, H.; Sahoo, Y.; Ohulchanskyy, T. Y.; Ding, Y.; Wang, Z. L.; Swihart, M.; Prasnad, P. N. *Nano Lett.* **2006**, *6*, 857.
(13) Mokari, T.; Sztrum, C. G.; Salant, A.; Rabani, E.; Banin, U. *Nat. Mater.* **2005**, *4*, 855.

Scheme 1. Influence of Crystal Structure on the Selective Growth of Metal[a]

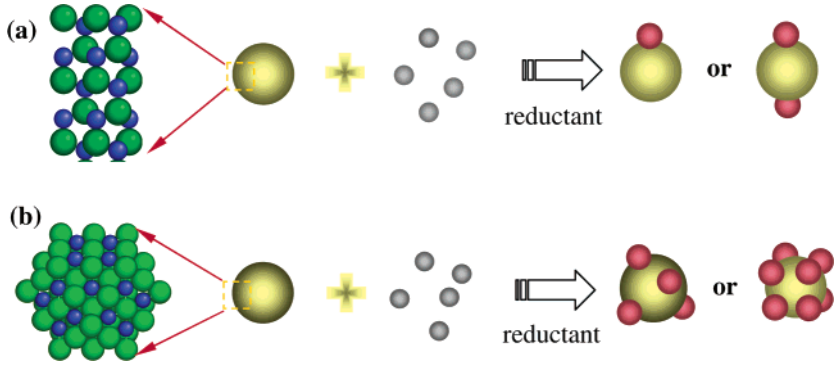

[a] (a) Reported nanostructures from the selective growth of metal on hexagonal-phase nanocrystals; (b) new nanostructures from the selective growth of metal on cubic-phase nanocrystals. Semiconductor, metal precursors, and metal are represented by yellow, gray, and red colors, respectively.

growth was attributed to the preferential nucleation of gold clusters on crystal facets with high reactivity. Since the reactivities of crystal facets are closely associated with crystal structures, the use of different crystal structures as the "growth substrates" may produce new and insightful results. Compared with hexagonal-phase crystal structures, cubic-phase crystal structures exhibit a higher symmetry and offer additional materials selection for applications. The preferential deposition of metal on cubic-phase nanocrystals leading to new and highly symmetrical nanostructures is visualized in Scheme 1b. These heterogeneous nanostructures may additionally self-assemble into ordered arrays, a property highly desirable for the chemical and/or biological applications of heterogeneous nanostructures.[14] Herein, the preferential deposition of metal on cubic-phase nanocrystals and the self-assembly of the resulting heterogeneous nanostructures into ordered arrays is demonstrated for the PbS−Au system. PbS was selected as the target semiconductor because it has a typical cubic crystal structure and can easily be produced in controlled shapes and sizes.[15,16] High-quality and monodisperse PbS−Au_1, PbS−Au_4 nanostructures and PbS−Au_n nanocubes were obtained under appropriate experimental conditions. The PbS−Au_4 nanostructures and the PbS−Au_n nanocubes, in particular, could spontaneously organize into ordered arrays with different symmetries. Since theories have predicted that the semiconductor/metal composites could show an enhanced nonlinear response compared to the constituent semiconductors,[17] the nonlinear optical properties of the as-synthesized PbS−Au_4 heterogeneous nanostructure were examined in some detail.

Experimental Section

PbS Nanocrystals. PbS nanocrystals were prepared by a previously reported solution method.[15] In brief, 0.28 g of $PbCl_2$ and 5 mL of oleylamine were introduced to a three-necked round-bottom flask at room temperature. The reaction system was sealed, vacuumed, and then purged by N_2 for 1 h to remove oxygen and moisture. The solution was then heated to 90 °C to form the Pb−oleylamine complex. An hour later, 2.5 mL oleylamine solution of sulfur (21 mg) were quickly injected into the above solution. The resulting solution was heated to 210 °C and aged at that temperature for 1 h. After the solution cooled to room temperature, methanol was added to precipitate PbS nanocrystals followed by centrifugation. The solid product so-obtained could disperse very well in toluene.

PbS−Au_1 Nanostructures. A 0.1 mL aliquot of toluene solution of 20 mM $HAuCl_4$ and 50 mM tetraoctylamine bromide was added to 2 mL of 50 mM dodecylamine. The resulting gold mixture was stirred at room temperature overnight. At the same time a toluene solution of PbS nanocrystals was diluted until the absorbance of the solution at 500 nm was about 1.15. This was to ensure that the PbS concentration was kept the same in all experiments. A diluted solution of PbS nanocrystals (4 mL) was then introduced to a three-necked round-bottom flask. The reaction system was sealed, vacuumed, and purged by N_2 for 1 h. The solution was then slowly heated to 40 °C. After 30 min, the stock solution of gold was injected into the PbS solution. The reaction was allowed to proceed at that temperature for 1 h. The reaction was then stopped, and the solution was centrifuged at 16 000 rpm for 10 min. The recovered solid was redispersed in toluene and used directly for TEM or XRD characterizations.

PbS−Au_4 Nanostructures and PbS−Au_n Nanocubes. The preparations of PbS−Au_4 nanostructures and PbS−Au_n nanocubes were similar to that of PbS−Au_1 nanostructures except that the quantities of $HAuCl_4$ in the stock solution were adjusted to 0.2 mL for the PbS−Au_4 nanostructures and to 0.5 mL for the PbS−Au_n nanocubes. Thin films of PbS−Au_4 were produced by spin coating at room temperature and used for the measurement of nonlinear optical properties.

Materials Characterizations. Powder X-ray diffraction (XRD) measurements were carried out on a diffractometer equipped with graphite monochromatized Cu Kα radiation (λ = 1.541 78 Å). TEM images, high-resolution TEM (HRTEM) images, selected area electron diffraction (SAED) patterns, and X-ray energy-dispersive spectroscopy (EDS) analysis of nanostructures were taken on a transmission electron microscope (JEOL AEM 2010). UV−visible spectra of the nanostructures were obtained on a Shimadzu 2450 UV−visible spectraphotometer at room temperature. PbS and PbS−Au_4 nanocrystals were coated on cover glasses using a spin-coater (Model P6700, Cookson Electronics). The response times of thin films of PbS and PbS−Au_4 nanocrystals on glass were investigated by a femtosecond pump−probe technique at a wavelength of 700 nm. Laser pulses (220 fs) at a 1-kHz repetition rate were used to minimize the average power and to reduce accumulative thermal effects. The laser pulses were generated by a mode-locked Ti:Sapphire laser (Quantronix, IMRA), which seeded a Ti:Sapphire regenerative amplifier (Quantronix, Titan). The wavelength was selected to be 700 nm as the laser pulses passed through an optical parametric amplifier (Quantronix, TOPAS).

Results and Discussion

Figure 1 shows the representative TEM images and SAED patterns of the starting PbS nanocrystals and the as-synthesized PbS−Au_1 heterogeneous nanostructures. The TEM image under

(14) Cozzoli, P. D.; Manna, L. *Nat. Mater.* **2005**, *4*, 801.
(15) Joo, J.; Na, H. B.; Yu, T.; Yu, J. H.; Kim, Y. W.; Wu, F.; Zhang, J. Z.; Hyeon, T. *J. Am. Chem. Soc.* **2003**, *125*, 11100.
(16) Lee, S. M.; Jun, Y. W.; Cho, S. N.; Cheon, J. *J. Am. Chem. Soc.* **2002**, *124*, 11244.
(17) Neeves, A. E.; Birnboim, M. H. *J. Opt. Soc. Am. B* **1989**, *6*, 787.

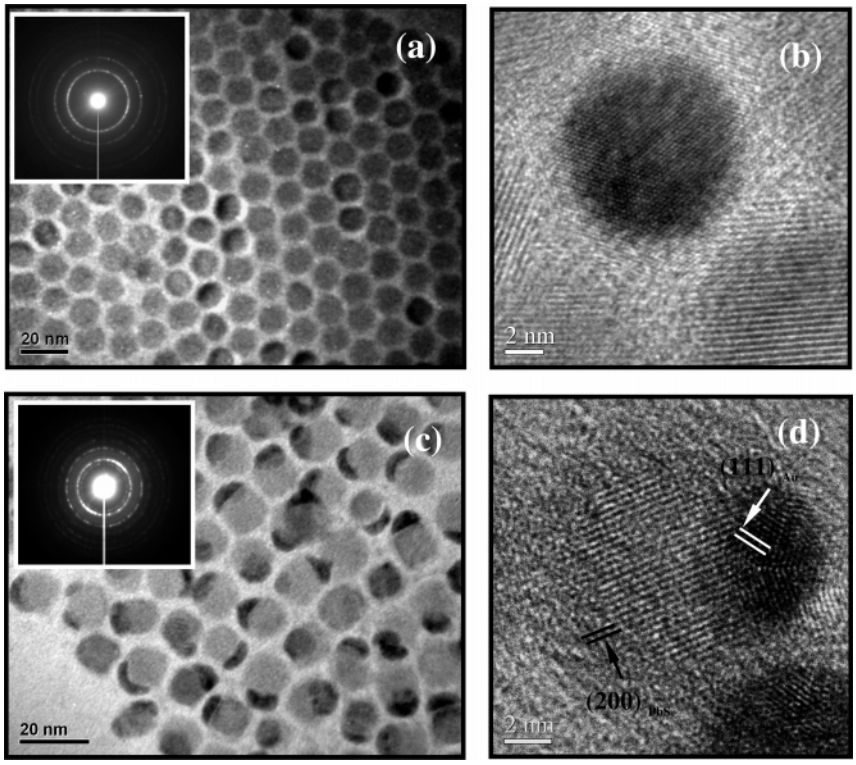

Figure 1. (a) TEM image and SAED pattern of the starting PbS nanocrystals; (b) HRTEM image of a typical PbS nanocrystal; (c) TEM image and SAED pattern of $PbS-Au_1$ heterogeneous nanostructures; (d) HRTEM image of a typical $PbS-Au_1$ nanocrystal. The subscript on Au is used to indicate the number of gold nanocrystals per semiconductor nanocrystal.

low magnification (Figure 1a) shows that the PbS nanocrystals were uniform spheres with an average diameter of approximately 12 nm. The SAED pattern of these nanocrystals (inset of Figure 1a) contains several distinctive diffraction rings which can be indexed as cubic-phase PbS. The HRTEM image (Figure 1b) of an individual nanocrystal shows clear and perfect crystal lattices throughout the entire crystal, indicating that the nanocrystal was single-crystalline in nature. This feature was important to the ensuing preferential deposition of gold nanocrystals.

All depositions of gold reported here were carried out under a fixed and excess amine concentration. When deposition was conducted under a low concentration of the gold salt (0.33 mM), uniform $PbS-Au_1$ heterogeneous nanostructures were the dominant product, as shown in Figure 1c. (The subscript on Au is used to indicate the number of gold nanocrystals on the surface of a semiconductor nanocrystal.) No isolated gold nanocrystals were found. This result indicates that the homogeneous nucleation of gold was well inhibited under the prevailing experimental conditions. Since gold has a strong imaging contrast, the dimeric nanostructure of the $PbS-Au_1$ composite could be easily identified. It is interesting to note that gold covered only one side of the PbS nanocrystals like a cap. The average size of PbS was almost unchanged at ~12 nm, and the height and diameter of the gold cap were about 3 and 7.6 nm, respectively. SAED (inset of Figure 1c) confirmed that the nanostructure was made up of crystalline PbS and Au. The diffraction rings from gold were rather weak because of the low volume fraction of gold in the nanostructure and of the defects introduced by the lattice mismatch at the Au−PbS interface. The crystalline nature of PbS and Au were also confirmed by the HRTEM image shown in Figure 1d. The lattice fringes in this figure could be indexed as the (200) crystal planes of PbS and the (111) crystal planes of Au. However, these crystal planes were not parallel to each other, and the angles between them varied from one nanocrystal to the next, indicating that the growth of gold took place in different orientations. This result is similar to a previous observation of the CdSe/Au nanostructure[13] but is different from the recent report on peanutlike PbS/Au nanostructure where the (200) crystal planes of PbS were parallel to the (111) crystal planes of gold.[12] This indicates that there was no epitaxial growth between the (200) planes of PbS and the (111) planes of Au.

If a moderate gold concentration (0.65 mM) was used in the deposition, the resulting nanostructures were found to spontaneously self-organize into ordered arrays up to several micrometers in size, as shown in Figure 2a. Fast Fourier Transformation (FFT) of the image (Figure 2g) showed hexagonal symmetry for the ordered array. It is believed that the narrow size distribution and symmetrical shape of the nanostructures promoted the formation of the ordered array. Upon closer examination (Figure 2b) the majority of these nanostructures were found to consist of a central PbS nanocrystal decorated with four gold nanocrystals. The four gold nanocrystals on the surface of PbS nanocrystals were not coplanar; instead they were spread out to form the vertices of a tetrahedron. Representative TEM images of this unique nanostructure are shown in Figure 2c and 2d. The regular placement of gold nanocrystals on the semiconductor implies that the deposition of gold was a highly selective process, which also prevailed in the formation of the $PbS-Au_n$ nanocubes (vida infra). The average sizes of PbS and gold nanocrystals were about 12 and 3 nm, respectively. While the PbS nanocrystals retained the size of the starting nanocrystals, the gold nanocrystals were smaller than those found in

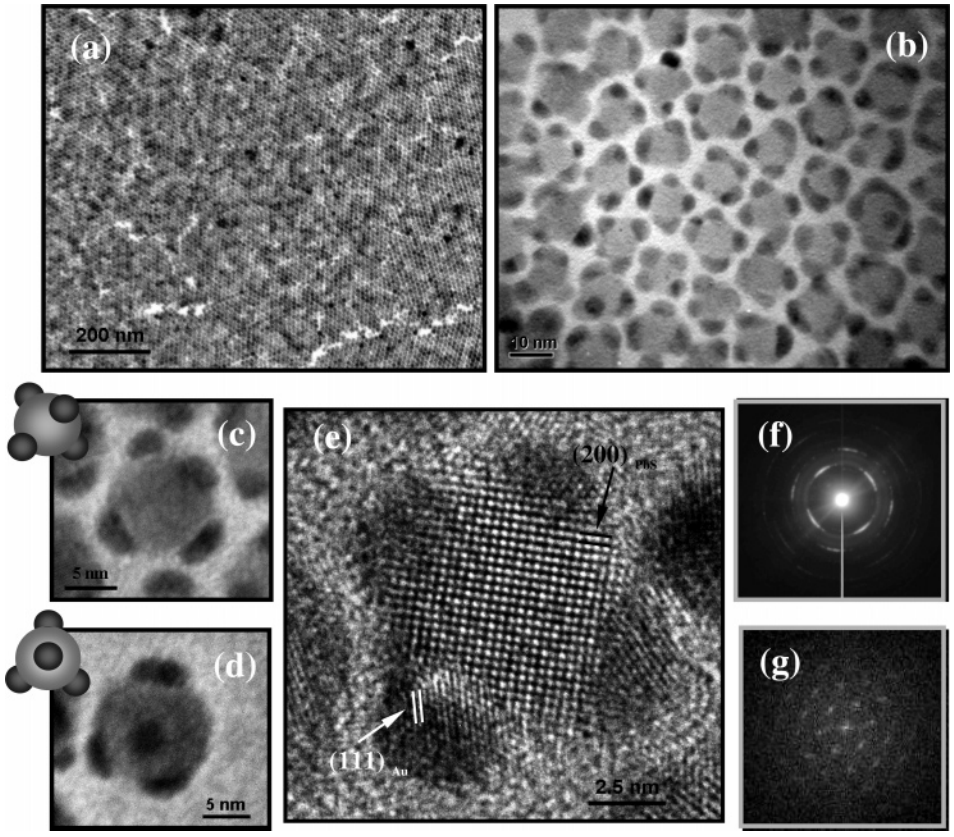

Figure 2. (a and b) TEM images of the ordered array of PbS−Au_4 heterogeneous nanostructures; (c and d) TEM images of a typical PbS−Au_4 nanostructure; (e) HRTEM image of a typical PbS−Au_4 nanostructure; (f) SAED pattern and (g) FFT pattern obtained from the ordered array of PbS−Au_4 heterogeneous nanostructures.

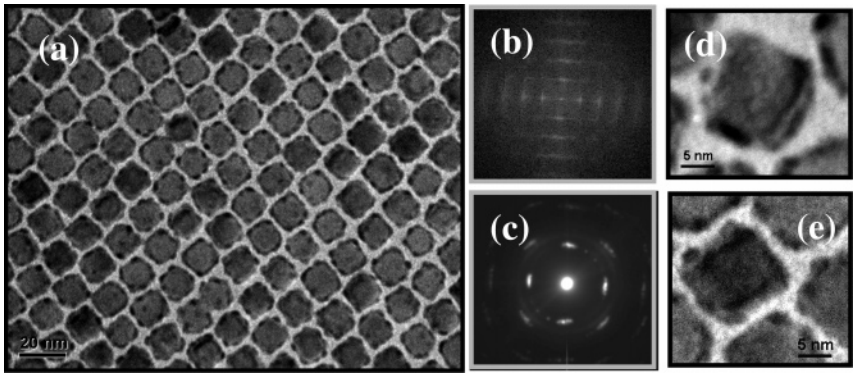

Figure 3. (a) TEM image of the ordered array of PbS−Au_n nanocubes; (b) FFT pattern and (c) SAED pattern obtained from the ordered array of PbS−Au_n nanocubes; (d and e) TEM images of a tilted PbS−Au_n nanocube.

PbS−Au_1 because of the increase in the number of gold nanocrystals. Figure 2e is the HRTEM image of the nanostructure showing clearly the lattice fringes of PbS and Au. Similar to PbS−Au_1, the PbS (200) planes were not parallel to the Au (111) planes, suggesting selective deposition by a nonepitaxial process. In addition to confirming the crystallinity of PbS and Au in the nanostructure, the SAED pattern in Figure 2f also shows four bright arcs on the same diffraction ring. This indicates that the semiconductor nanocrystals in the ordered array were preferentially oriented. EDS (Supporting Information) only picked up the presence of Pb, S, and Au, besides the background signals from C and Cu. The XRD pattern (Supporting Information) of the heterogeneous nanostructures could also be indexed as cubic-phase PbS and Au, corroborating the SAED measurements.

If the deposition of gold was conducted under a high concentration of the gold precursor (~1.54mM), an ordered array of PbS−Au_n nanocubes was formed (Figure 3a). Fast Fourier Transformation of the TEM image (Figure 3b) revealed tetragonal symmetry, which is significantly different from the hexagonal symmetry obtained from the ordered arrays of PbS−Au_4 nanostructures. The finding that the symmetry of ordered arrays was determined by the shape of the building blocks is in agreement with the theoretical prediction.[17] The SAED pattern (Figure 3c) also contains the same features as those in PbS−Au_4. The size of the nanocubes was slightly larger than the size of the starting PbS nanocrystals due to the attachment of the gold nanocrystals. To determine the distribution of gold on the semiconductor, TEM images of titled nanocubes were taken (Figure 3d and 3e). The congregation of gold nanocrystals along

Scheme 2. Evolution of Heterogeneous Nanostructures Resulting from the Preferential Deposition of Gold on PbS Nanocrystals, as the Concentration of $HAuCl_4$ Increases[a]

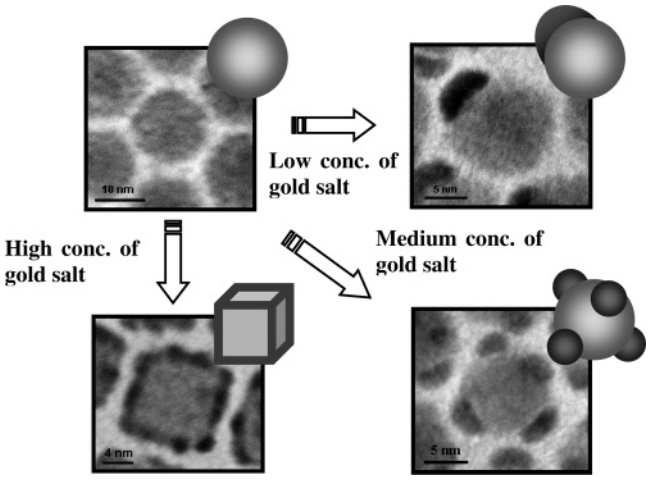

[a] Semiconductor and metal are colored by light gray and dark gray, respectively.

the ridges of the nanocubes showed up as black edges in the TEM images. The unique arrangement of gold on the surface of semiconductor nanocrystals confirms again the selective nature of the gold deposition process.

The selective deposition of gold on PbS nanocrystals may be understood as follows: At low gold precursor concentration, there was insufficient gold in the solution to support multiple nucleation on the same PbS nanocrystal. Therefore, Au distributed uniformly among the available PbS nanocrystals resulting in one Au nanocrystal per PbS nanocrystal. The probability of forming multiple nucleations on the same PbS nanocrystal increased at an intermediate gold precursor concentration due to enhanced kinetics of Au reduction which consequently led to a corresponding increase in the number of embryonic Au clusters in the solution. It is well-known that reactivity is different on different crystal facets, particularly in the presence of ligands (amine in our case). The deposition of gold should therefore occur preferentially on PbS facets with the highest reactivity. In the cubic crystal system, the growth rates on common crystal planes as regressed from previous works on various nanostructures can be ordered as [111] > [110] > [100].[15] This suggests that Au would preferentially grow on the {111} facets. Because of the different polarities of the (111) and $(\bar{1}\bar{1}\bar{1})$ facets, only four of the {111} facets were deposited and the PbS−Au_4 nanostructure was formed. A similar phenomenon has been observed in the growth of semiconductor tetrapods.[19] At high gold precursor concentration, gold would saturate all the {111} facets and PbS−Au_8 should be formed. The existence of the PbS−Au_8 nanostructure had been confirmed experimentally (Supporting Information), although the yield of this nanostructure under the experimental conditions was rather low. At an even higher gold precursor concentration, the surfactant in the gold solution (tetraoctylammonium bromide) was found to alter the shape of PbS nanoparticles from spheres to cubes (Supporting Information). Because vertexes and edges of nanocrystals are more reactive than the facets,[20]

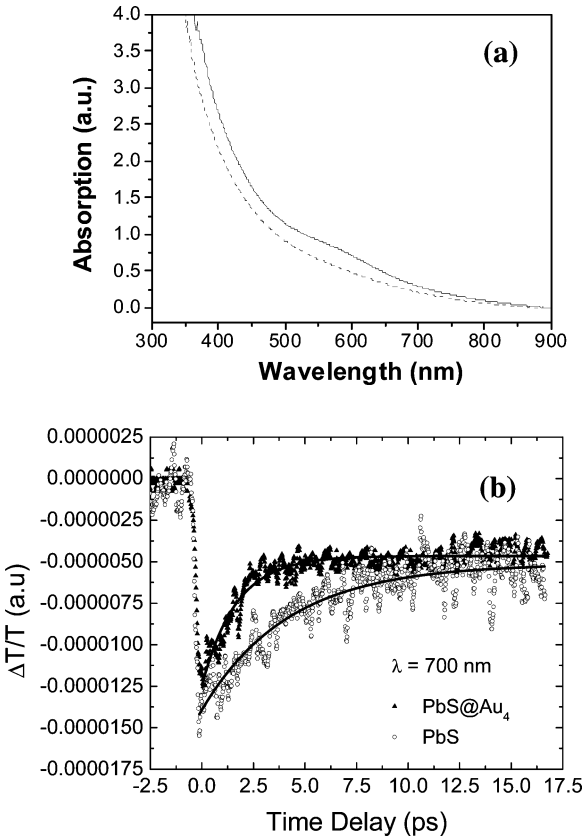

Figure 4. (a) UV−vis spectra of PbS nanocrystals (solid line) and PbS@Au_4 heterogeneous nanostructures (dash line). (b) Degenerate 220-fs-time-resolved pump−probe measurements of the PbS and PbS−Au_4 nanocrystalline thin films performed at 700 nm with pump irradiance of 15.0 GW/cm^2. The solid lines are best-fit curves using a biexponential function.

they were the sites for preferential Au deposition, forming the resultant gold-crowned cubic-shaped heterogeneous nanostructure. The growth process is summarized schematically in Scheme 2. Since the deposition of gold depended on the reactivity of the crystal planes, there was no need for the deposition to conform to the requirements of epitaxial growth, and the two crystal lattices could therefore orient differently from each other.

The optical properties of the nanostructures were examined with an emphasis on the PbS−Au_4 system because such a unique structural feature has not been previously reported. The optical absorption of PbS−Au_4 was measured in the range of 300−900 nm at room temperature, and the resulting spectrum is shown in Figure 4a. The absorption due to gold nanoparticles was not apparent in this spectrum, which is quite different from the results of Prasad et al.[12] The difference could arise from the small size of the gold nanoparticles (~3 nm) and the low Au/PbS ratio in the heterogeneous nanostructure, causing the absorption by the gold nanoparticles to be overshadowed by the more prominent PbS absorption. Comparison with the absorption spectrum of pure PbS nanoparticles, however, showed the disappearance of a shoulder around 550 nm which may be taken as an indirect indication for the presence of gold in the heterogeneous nanostructure. The luminescence properties of the semiconductor-metal nanoparticles from the charge transfer between Au and PbS fall in the IR region, which is beyond the measurement capability of our instrumentation.

(18) Yamamuro, S.; Sumiyama, K. *Chem. Phys. Lett.* **2006**, *418*, 166.
(19) Manna, L.; Milliron, D. J.; Meisel, A.; Scher, E. C.; Alivisatos, A. P. *Nat. Mater.* **2003**, *2*, 382.
(20) Pong, B. K.; Lee, J. Y.; Trout, B. L. *Langmuir* **2005**, *21*, 11599.

Figure 4b shows the transient absorption signals of PbS and PbS−Au_4 nanocrystal thin films. The pump irradiance was setup at 15.0 GW/cm^2 to allow for reverse saturable absorption (RSA) in the PbS nanocrystals.[21] The pump−probe measurements revealed that the photoexcited electron dynamics in PbS nanocrystals was dominated by two relaxation processes: the fast (3.5 ps) and the slow (29 ps) decay components. The fast dynamics is commonly attributed to exciton−exciton annihilation upon trap state saturation at high excitation intensities, whereas the slow dynamics is attributed to an electron−hole combination for deep trap states.[22] The deep states in the band gap are related to excess Pb atoms at the interface of PbS nanocrystals. The corresponding response times for the PbS−Au_4 nanostructure obtained by fitting the experimental data with a biexponential function were 2.5 and 35 ps, respectively. The experimental results indicate that the presence of Au in the PbS−Au_4 nanostructure had reduced the response time of the fast component (by ∼1 ps or 29%) and lengthened the response time of the slow component (by ∼6 ps or 21%). Au-induced electron−phonon and phonon−phonon interactions could have been the cause. In addition, the carrier shift between Au nanocrystals and PbS nanocrystals might also be involved, which deserves further investigations. The measured optical properties suggest that PbS−Au_4 nanocrystals can be used as saturable absorber devices.

Conclusions

In summary, a facile solution route to producing high-quality, monodisperse PbS−Au_1, PbS−Au_4, and PbS−Au_n nanostructures has been developed. The formation of these nanostructures was based on the difference in polarity of crystal facets that led to the growth of metal on a semiconductor surface in selective directions. This method provides a reasonable method to control the size, number, and distribution of metal nanocrystals on semiconductors, which is important to the design and fabrication of composite nanomaterials for catalysis, optoelectronic devices, and chemical/biological sensors. Owing to their narrow size distribution and intrinsic high symmetry, the as-synthesized PbS−Au_4 heterogeneous nanostructures could easily self-assemble into hexagonal arrays. Besides the PbS−Au_4 nanostructure, PbS−Au_n nanocubes could also be formed and used to generate square arrays. These unique heterogeneous nanostructures and their ordered arrays are, to the best of our knowledge, hitherto unreported. Nonlinear optical measurements showed that the PbS−Au_4 nanostructure could alter the nonlinear response time of PbS nanocrystals, thereby confirming the applicability of metal-decorated semiconductor nanocrystals in the development of saturable absorber devices.

Acknowledgment. The authors gratefully thank Singapore-MIT Alliance for its financial support on this project. J.Y. also appreciates the assistance from Mr. Phai Ann Chai and Zhenghua Shuang on TEM measurements.

Supporting Information Available: EDS spectrum and XRD pattern of the PbS−Au_4 nanostructure; TEM images of the as-prepared PbS−Au_8 hetero-nanostructure. These materials are available free of charge via the Internet at http://pubs.acs.org.

JA062494R

(21) Buso, D.; Falcaro, P.; Costacurta, S.; Guglielmi, M.; Martucci, A.; Innocenzi, P.; Malfatti, L.; Bello, V.; Mattei, G.; Sada, C.; Amenitsch, H.; Gerdova, I.; Hache, A. *Chem. Mater.* **2005**, *17*, 4965.
(22) Patel, A. A.; Wu, F.; Zhang, J. Z.; Torres-Martines, C. L.; Mehra, R. K.; Yang, Y.; Risbud, S. H. *J. Phys. Chem. B* **2000**, *104*, 11598.